

# Spatially Confined CVD Growth of High-Density Semiconducting Single-Walled Carbon Nanotube Horizontal Arrays

Liu Qian, Qian Shao, Yue Yu, Weiming Liu, Shanshan Wang, Enlai Gao, and Jin Zhang\*

High-density horizontally aligned single-walled carbon nanotube (SWNT) arrays with high-purity semiconducting tubes are promising materials for energy-efficient electronics. However, realizing high density and high semiconducting purity through the direct-growth method is still a challenge. Here the problem is overcome through a spatially confined approach based on a floating solid catalyst chemical vapor deposition (FSCVD) system. A confined space is designed to change the fluid dynamics in a chemical vapor deposition reactor, offering a trapping effect for both catalyst nanoparticles and carbon fragments. Therefore, densely and uniformly distributed catalyst nanoparticles are continuously deposited on substrates, greatly increasing the growth probability and efficiency of SWNTs. Besides, the solid catalyst TiC and the oxygen-vacancy-enriched catalyst TiO both facilitate the growth of semiconducting tubes. As a result, SWNT horizontal arrays with a high density of 65 tubes  $\mu\text{m}^{-1}$  and a semiconducting purity of >95% are realized, which hold the potential for future application in carbon nanotube electronics.

## 1. Introduction

Single-walled carbon nanotubes (SWNTs) are promising for future application in highly-integrated electronics because of their nanoscale sizes and excellent electrical properties.<sup>[1–3]</sup> Based on horizontally aligned SWNT arrays, field effect transistors (FETs) that outperformed commercial silicon FETs with

similar gate lengths have been reported,<sup>[4]</sup> and a carbon nanotube (CNT) computer running a basic operating system has been successfully developed.<sup>[5]</sup> However, the SWNT arrays now available for device are still far from being ideal due to their diverse structures, which has become a bottleneck for their real application.

In an SWNT based FET, the channel requires enough parallel SWNTs to drive the demand current, and a high purity of semiconducting SWNTs (s-SWNTs) to ensure the switching characteristic.<sup>[6]</sup> The aligned SWNT arrays used in the aforementioned high-performance FETs and computers were processed through solution separation<sup>[4]</sup> or electrical breakdown,<sup>[5]</sup> which brought inevitable damage or impurity to the SWNT materials. The residual polymers in solution-processing methods lead to poor contacts between


CNTs and electrodes, thus decreasing the device performance.<sup>[4]</sup> Therefore, direct growth of SWNT arrays with high density and high purity of s-SWNTs is an ideal way to break the bottleneck. Great efforts have been made in the study of chemical vapor deposition (CVD) growth of aligned SWNT arrays. Through multi-loading of catalysts<sup>[7]</sup> or multiple CVD growth methods,<sup>[8]</sup> SWNT arrays with density of 20–70 tubes  $\mu\text{m}^{-1}$  were achieved, and ultrahigh-density of up to 130–160 tubes  $\mu\text{m}^{-1}$  was directly realized using Trojan catalysts,<sup>[9–10]</sup> but these arrays exhibited almost no selectivity for s-SWNTs. On the other hand, although SWNTs arrays with high purity of semiconducting tubes (95–99.9%)<sup>[11–13]</sup> or even specific chirality (>90%)<sup>[14,15]</sup> were obtained, these arrays were usually of low densities. Therefore, realizing high density and high semiconducting purity at the same time is still a challenge.

The difficulty of realizing structure control in high-density arrays lies in the difficulty of obtaining high-density catalyst nanoparticles with specific structures and uniform sizes. In our previous work, a floating solid catalyst CVD (FSCVD) strategy was developed to continuously obtain solid catalyst nanoparticles in gas phase through decomposition and reaction of catalyst precursor in carrier gas.<sup>[16]</sup> The obtained FSCs can be deposited on any substrates and further used to grow SWNT arrays with specific chirality. However, after systematical optimization, the density of the array was still limited because of the relatively low catalytic activity of titanium carbide (TiC) catalysts and a low deposition efficiency of nanoparticles

L. Qian, Y. Yu, W. M. Liu, S. S. Wang, J. Zhang  
Center for Nanochemistry  
Beijing Science and Engineering Center for Nanocarbons  
Beijing National Laboratory for Molecular Sciences  
College of Chemistry and Molecular Engineering  
Peking University  
Beijing 100871, P. R. China  
E-mail: jinzhang@pku.edu.cn

Q. Shao, E. L. Gao  
Department of Engineering Mechanics  
School of Civil Engineering  
Wuhan University  
Wuhan, Hubei 430072, P. R. China

J. Zhang  
School of Material Science and Engineering  
Peking University  
Beijing 100871, P. R. China

 The ORCID identification number(s) for the author(s) of this article can be found under <https://doi.org/10.1002/adfm.202106643>.

DOI: 10.1002/adfm.202106643

under high temperature. Therefore, apart from basic growth condition, the gas flow dynamics in CVD reactors must be taken into consideration since the floating of catalysts offers a chance to adjust the behaviors of catalyst nanoparticles in gas phase. Changing reaction space is an effective way to change the fluid model, and decreasing the space to a certain size has emerged as an effective way for the growth of high-quality 2D materials.<sup>[17–19]</sup> Specially, the decreased space may result in a trapping effect for useful reagents and improving the reaction efficiency.<sup>[17]</sup> Herein, based on titanium (Ti)-FSCCVD system, we developed a spatially confined strategy to effectively improve the density of horizontally aligned SWNT arrays with designed structures. The confined space (<10 μm) traps both catalysts and carbon fragment, leading to a higher efficiency of catalyst deposition and SWNT growth. Moreover, the catalyst structures of the solid TiC crystal and the oxygen-vacancy-enriched titanium oxide (TiO) contributed to the growth of s-SWNTs. Therefore, high-density SWNT arrays of up to 65 tubes μm<sup>-1</sup> on quartz substrates with >95% purity of s-SWNTs were obtained.

## 2. Results and Discussion

### 2.1. Growth of High-Density SWNT Arrays

The confined space was set by placing an ST-cut quartz upside down onto another substrate with their polished surfaces face to face (Figure 1a). Because of the surface topography,<sup>[20]</sup> a gap of <10 μm was formed when using Si/SiO<sub>2</sub> (300 nm) as the supporting substrate (Figure S1a, Supporting Information). The

narrow gap can be further decreased by exerting pressure onto the quartz substrate. The stacked-up substrates were then put into a Ti-FSCCVD system to grow SWNTs (Figure 1a). The catalyst deposition and SWNT growth procedure are similar to the previous report.<sup>[16]</sup> Specially, we introduced ferrocene into the furnace as a catalyst promoter to increase the decomposition efficiency of the carbon feedstock. The catalyst promoter was carried by a small flow (50 sccm) of argon gas under room temperature. After growing for about 40 min, horizontally aligned carbon nanotube array was obtained on the quartz substrate. As shown in Figure 1b,c, a uniform, highly oriented carbon nanotube array with high density was observed by scanning electron microscope (SEM). In the atomic force microscopy (AFM) image in Figure 1d, the highest density of the array was measured to be 65 tubes μm<sup>-1</sup>.

### 2.2. The Influence of Confined Space and Growth Temperature

In order to figure out the influence of the small gap, we compared the growth results on quartz substrates without and with gaps of different sizes. As shown in Figure 2a and Figure S2a (Supporting Information), when the quartz substrate was put face up in the CVD system (exposed to the reaction atmosphere), the as-grown carbon nanotubes were sparse and with a lot of large particles, which originated from sintering and aggregation of catalysts with carbon wrapped. The introduction of catalyst promoter ferrocene may cause the deposition of carbon on large catalyst particles. When the quartz substrate was put onto another quartz substrate with their polished surfaces

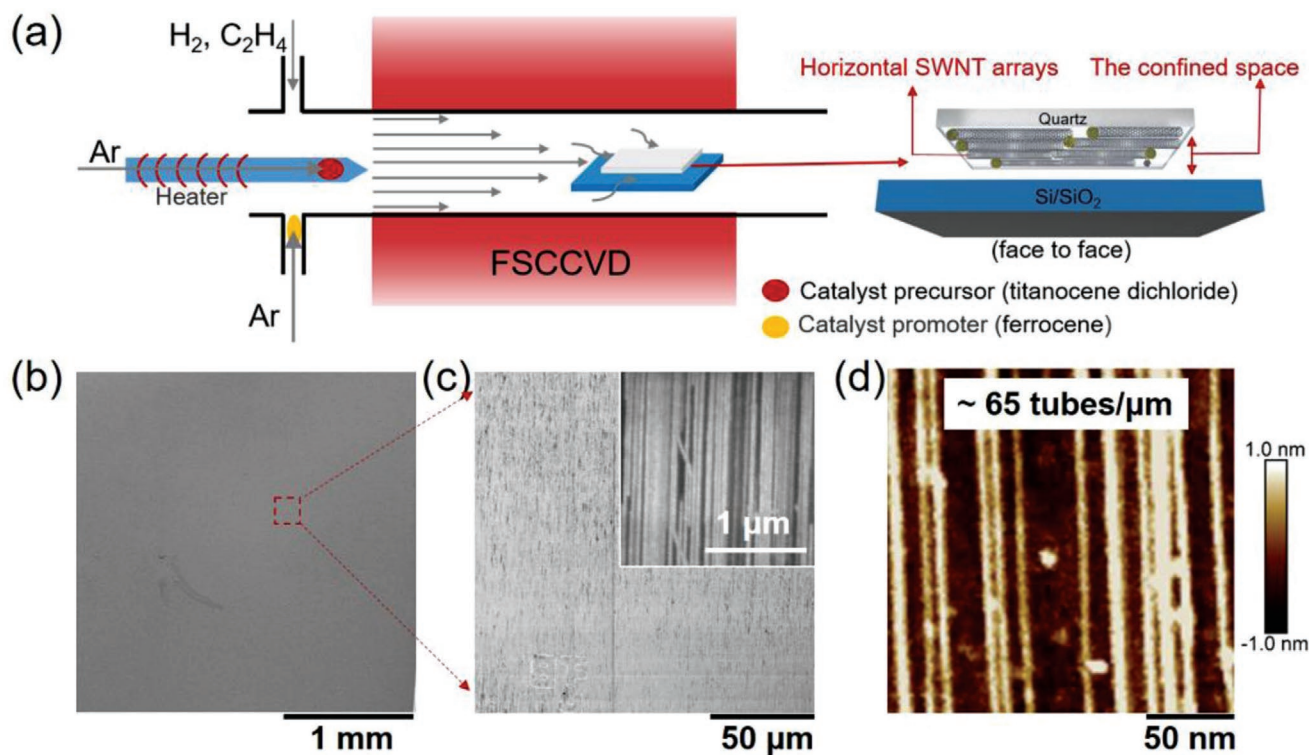


**Figure 1.** Growth of high-density SWNT arrays. a) Schematic showing the spatially confined CVD growth method. b,c) SEM images of the as-grown SWNT array at different magnifications. d) A typical AFM image of the high-density SWNT array showing a density of 65 tubes μm<sup>-1</sup>.

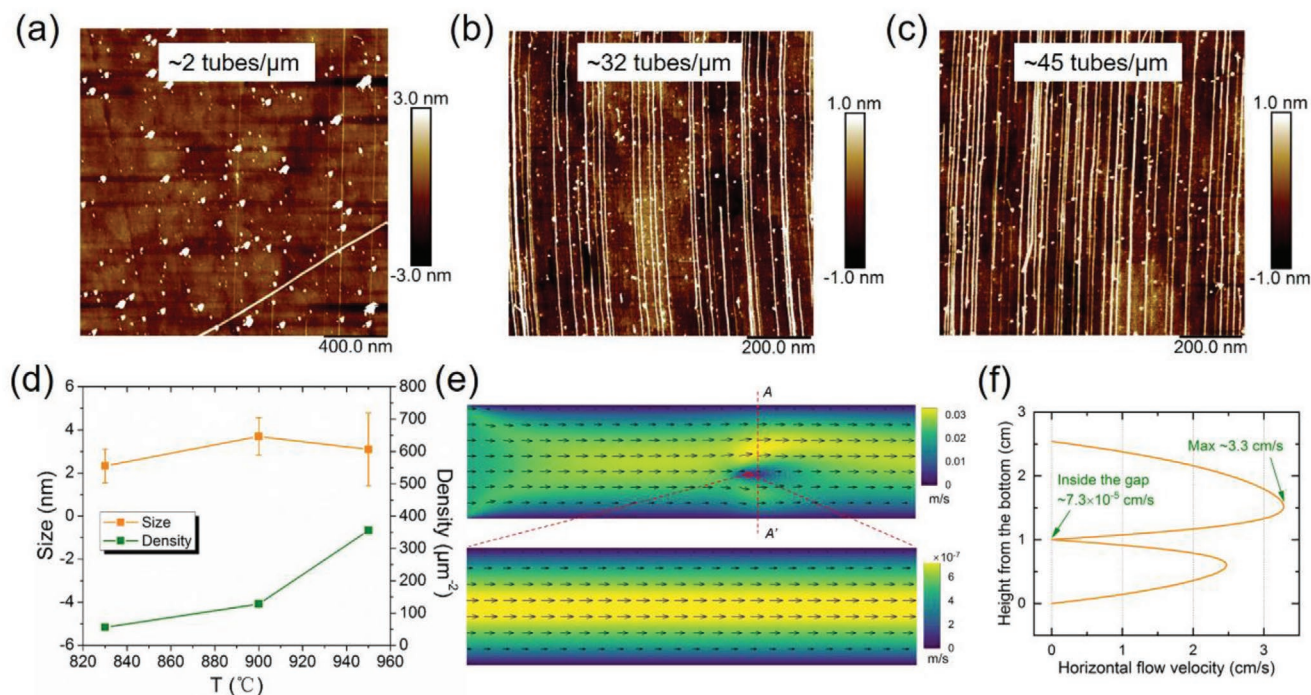


**Figure 2.** Mechanisms for growth of high-density SWNT arrays in confined space. a) A typical AFM image of catalyst nanoparticles and as grown SWNTs on quartz substrates without confined space. b,c) AFM images of SWNT arrays grown in confined space built by b) quartz-Si/SiO<sub>2</sub> substrates and c) quartz-Si/SiO<sub>2</sub> substrates with a weight. d) Statistics showing the changes of nanoparticles sizes and densities with temperatures. e) Flow velocity field in the tube with a narrow gap. f) Velocity profile at the dash line of the tube as illustrated in (e).

face to face, there was a gap of  $\approx 30 \mu\text{m}$  (Figure S1b, Supporting Information). The morphology of the as-grown SWNT array was similar to that without a gap, with a density of only  $\approx 1 \text{ tube } \mu\text{m}^{-1}$  (Figure S2b, Supporting Information). When the supporting substrate was changed to Si/SiO<sub>2</sub>, the gap between the two substrates was decreased to  $< 10 \mu\text{m}$ , and two weights made from quartz were used as pressure to further decrease the gap. The SEM images in Figure S2b–d (Supporting Information) demonstrated that the densities of the arrays increased greatly with the decreasing sizes of the gaps. However, when the gap was too narrow (Figure S2e, Supporting Information), a large amount of amorphous carbon was found on the quartz substrate, and the number of carbon nanotubes was greatly reduced. Therefore, we further optimized the growth condition for stacked quartz-Si/SiO<sub>2</sub>, and SWNT arrays with average densities of  $32 \text{ tubes } \mu\text{m}^{-1}$  and  $45 \text{ tubes } \mu\text{m}^{-1}$  were obtained without and with only one weight, respectively (Figure 2b,c). Besides, the catalyst nanoparticles were smaller-sized with higher density and better distribution. Figure S3 (Supporting Information) shows more AFM images of the best array at different positions on the substrate and the diameter distribution of the tubes.

To study the influence of gas kinetics on SWNT growth, the couples of substrates were put at three different positions in the reactor tube, which were measured to be 950, 900, and 830 °C, respectively. The SWNT arrays grown under different temperatures were shown in Figure S4 (Supporting Information), which demonstrated the highest density at 900 °C. Then the size distributions and densities of the deposited catalyst nanoparticles

at three different temperatures were statistically analyzed, and the original AFM images and statistics were shown in Figure S5 (Supporting Information). The results (Figure 2d) revealed that a higher temperature caused a higher density of nanoparticles, but a wider size distribution, which contained a lot of large particles not suitable for SWNT growth (Figure S5a, Supporting Information). Besides, a high temperature of 950 °C may cause the excessive decomposition of carbon feedstock, leading to the poisoning of catalysts and fewer SWNTs.<sup>[21]</sup> At 900 °C, the catalyst nanoparticles had a narrow size distribution with an average size of  $\approx 3.7 \text{ nm}$  (Figure S5c, Supporting Information). The particles obtained under a relatively low temperature had a smaller average size, but a low density, which also led to a low density of SWNTs (Figure S5e, Supporting Information). Therefore, compared with the growth result without small gaps, a better distribution of catalyst nanoparticles is one of the key factors for high-density SWNT array growth. The density of the catalyst nanoparticles and the catalyst activity of a certain nanoparticle should be considered together when pursuing high densities in SWNT arrays.

### 2.3. Mechanisms for the Growth of High-Density SWNTs

To understand the growth behaviors of SWNTs in small gaps, we propose a confinement-induced diffusion model. In our CVD growth system, the height of the gap ( $h \approx 10 \mu\text{m}$ ) is over three orders of magnitude less than the diameter of the tube ( $D = 2.54 \text{ cm}$ ). Based on the theory of fluid dynamics, the flow



velocity through the gap ( $V_{\text{gap}}$ ) is expected much slower than that through the tube ( $V_{\text{tube}}$ ). To quantify the difference, we conducted computational fluid dynamics simulations as shown in Figure 2e,f. It shows that the maximum flow velocity in the gap is about  $7.3 \times 10^{-5} \text{ cm s}^{-1}$ , while the averaged flow velocity in the tube is  $2.0 \text{ cm s}^{-1}$ , indicating more than  $10^4$  times reduction of flow velocity from the tube to the narrow gap. It means that the fastest time required for the gas flow through the gap (length of 0.6 cm) is  $8.2 \times 10^3 \text{ s}$  by flow dynamics. On the other hand, we estimated that the time scale for an ethylene molecule diffusing through the gap ( $t$ ) was about 0.18 s (for details see the Supporting Information). This diffusion time scale is much smaller than the time for gas flowing through the gap. Hence, it can be concluded that the diffusion of gas molecule and nanoparticles dominates the molecular motion in the gap. Additionally, the increase of temperature can further enhance the diffusion behaviors.

Based on the diffusion model, the behaviors of the reaction gas and the catalysts can be explained. For ethylene gas, the molecules were trapped in the gap because of longer diffusion time on substrates than that exposed directly to tube atmosphere. The longer dwell time facilitated a more complete decomposition of carbon feedstock and reaction between carbon fragments and catalyst nanoparticles. For catalyst nanoparticles, the precursor – titanocene dichloride – decomposed and gradually carbonized with the increasing temperature, and entered into the small gap with the diffused carrier gas. We hypothesize a certain probability for a nanoparticle to deposit on the substrate when colliding with the substrate, that is, one of the gap walls. The average number for a nanoparticle colliding with the gap walls ( $n$ ) in the process of traveling out of the gap is determined by

$$n = \frac{t}{\frac{1}{f} \left(\frac{h}{\lambda}\right)^2} = \left(\frac{l}{h}\right)^2 \quad (1)$$

where  $f$  is the collision frequency between nanoparticles and  $l$  is the length of the substrate aligning the gas flow direction. Therefore, it can be found that  $n$  increases with the decrease of  $h$ , and the increase of catalyst colliding with the substrate will greatly increase the deposition probability of the catalyst nanoparticles on substrates and reduce the particle aggregation in gas phase. This is consistent with our experimental result that as the size of the gap  $h$  decreased, the density of the nanoparticles increased (Figure 2a–c), which provides the necessary condition for high-density SWNT array growth.

The small gap actually “traps” the carbon fragments and catalysts, resulting in higher-density catalyst nanoparticles that have the activity to grow SWNTs and higher reaction probability and efficiency. Therefore, the method is named as spatially confined CVD growth. When the temperature is changed, the average velocity of nanoparticles increases with the increasing temperature, and the number of nanoparticles that diffuse into the confined space increases. At a proper temperature, the nanoparticles have high density, uniform distribution and suitable size, which is consistent with our experimental results (Figure 2d).

#### 2.4. Growth of SWNT Arrays with High Semiconducting Purity

Through ferrocene-promoted FSCCVD method and spatially confined growth, we realized continuously loading of catalysts and high-efficiency growth of SWNTs. To explore the structure control of the designed catalysts over SWNT growth, transmission electron microscope (TEM) was used to identify the structure of the catalyst nanoparticles. A  $\text{SiN}_x$  (10 nm) grid was put upside down onto a  $\text{Si}/\text{SiO}_2$  substrate and used as the substrate to grow carbon nanotubes in Ti-FSCCVD system. As shown in Figure 3a, three catalyst nanoparticles were detected in the annular dark field scanning transmission electron microscopy (ADF-STEM) image. The corresponding energy dispersive spectrometer (EDS) mapping images (Figure S6, Supporting Information) and spectrum (Figure 3b) demonstrate that the nanoparticles are titanium-based compounds. X-ray photoelectron spectroscopy (XPS) measurement was conducted to confirm the coposition of the catalysts (Figure S7, Supporting Information). Ti–C bonds in both Ti 2p spectrum and C 1s spectrum indicated the formation of TiC under the growth atmosphere. Besides, titanium oxides ( $\text{TiO}_x$ ) were also detected.

High-resolution TEM (HRTEM) image of a typical catalyst nanoparticle is demonstrated in Figure 3c, which is obviously separated into two parts (marked by two different colors). Figure 3d,e are the fast Fourier transform (FFT) images corresponding to the two parts, respectively. The lattice plane indexes marked on the reflection spots were calculated by the interplanar spacing measured in the reciprocal space ( $d_{(0\ 0\ 2)} = 0.22 \text{ nm}$ ,  $d_{(1\ 1\ 1)} = 0.25 \text{ nm}$ ,  $d_{(2\ 2\ 0)} = 0.15 \text{ nm}$ ), which match well with those of the face-centered cubic structure of TiC or TiO crystal diffracted along the zone axis of  $\langle 1\bar{1}0 \rangle$ . Combining the HRTEM analysis with the EDS and XPS results mentioned above, it can be deduced that the catalyst nanoparticle is either TiC or TiO. More HRTEM images of the catalyst nanoparticles are shown in Figure S8 (Supporting Information), indicating the same crystal structures. Compared with FSCCVD system without confined space, the introduction of oxygen during the catalyst formation process might arise from the oxygen release from the oxide substrate, which is also beneficial for the decomposition of carbon feedstock.<sup>[17]</sup> The appearance of other titanium oxides in XPS (Figure S7, Supporting Information) might be derived from the oxidation of nanoparticles in air before test.

It is worth noting that no iron (Fe) signal was detected through the EDS mapping (Figure 3b; Figure S7, Supporting Information), which means that the introduction of ferrocene doesn't lead to the Fe deposition or carbon nanotube growth. The decomposed Fe worked as a catalyst promoter in gas phase to increase the catalytic activity of Ti-based catalysts, and flowed out with the carrier gas. The influence of ferrocene on SWNT growth is shown in Figure S9 in the Supporting Information.

Although the catalysts are actually two titanium compounds, the structure-controlled growth of SWNTs can also be predicted because of the specific structures of the two catalysts. Using TiC as catalysts, it has been proved that SWNTs with fourfold symmetry, mainly (16, 8) and (12, 8) tubes, are preferential to grow because the (2 0 0) plane of TiC crystal has fourfold symmetry.<sup>[16]</sup> As for TiO crystals, they are actually stable crystals with a high number of oxygen vacancies,<sup>[22]</sup> which were also proved to provide a lower formation energy for s-SWNT

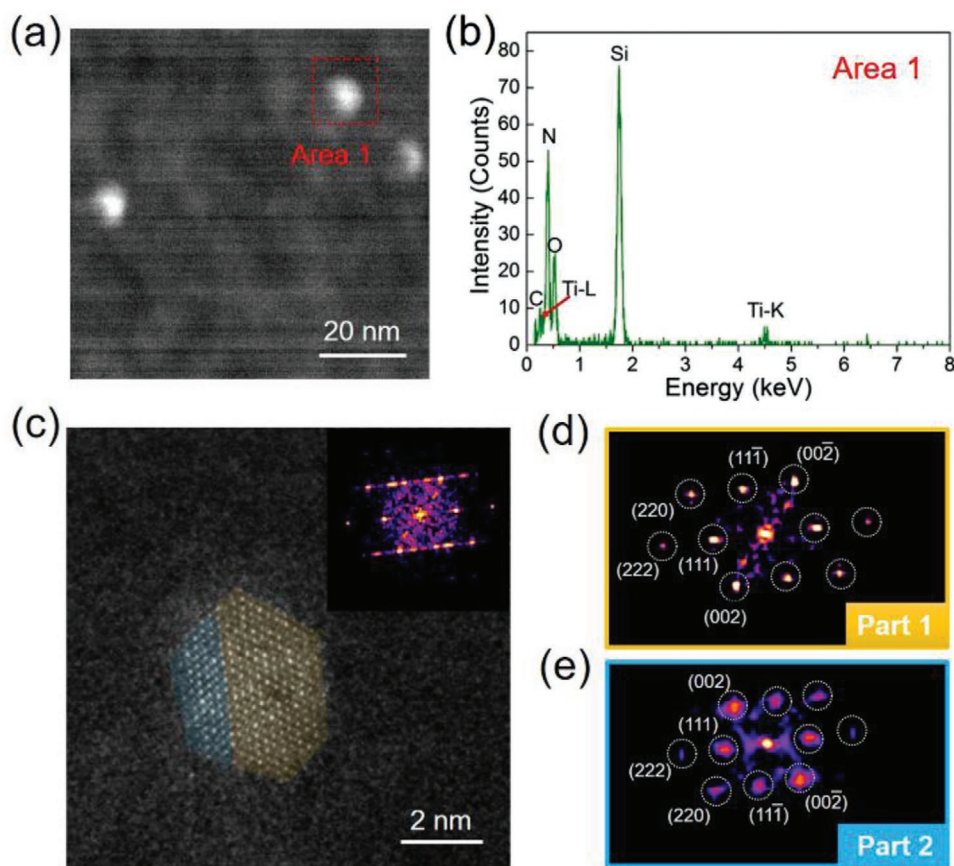


**Figure 3.** TEM characteristics of catalyst nanoparticles. a) ADF-STEM image of three catalyst nanoparticles. b) EDS spectrum for Area 1 in (a) showing no Fe signal. c–e) A typical HRTEM image of a catalyst nanoparticle and corresponding FFT patterns for the d) part 1 (yellow) and e) part 2 (blue) of the nanoparticle.

nucleation.<sup>[23]</sup> Raman line mapping measurements excited by four different lasers (wavelengths of 488, 532, 633, and 785 nm) were performed to investigate the structures of the SWNTs after transferring the arrays to Si/SiO<sub>2</sub> (90 nm) substrates (inset of **Figure 4a**). **Figure 4a** demonstrated the Raman line mapping spectra of the high-density SWNT arrays under 532 nm laser excitation, with RBM, G bands and barely D bands, indicating high qualities of the SWNTs. The RBM regions excited by four excitation lasers and obtained from more than three parallel samples are shown in **Figure 4b–e** (for full Raman spectra see **Figure S10** in the Supporting Information). The RBM peaks are apparently concentrated in the region of semiconducting tubes. The statistics shows that among all the 559 RBM peaks that detected, only 30 belong to metallic tubes, indicating an s-SWNT purity of  $\approx 95\%$  (**Table S1**, Supporting Information). Besides, back gate field-effect transistors (FETs) based on the high-density SWNT arrays were fabricated to perform the electrical measurements. **Figure 4f** is the transfer curve of a typical FET with channel length of 1  $\mu\text{m}$  and width of 30  $\mu\text{m}$  (inset is the SEM image for the channel of the device). The device showed an on/off ratio of  $\approx 3 \times 10^3$ , indicating the semiconducting properties of all the effective tubes in the channel. Because of the high density, bundles of SWNTs might appear after the wetting transfer process. A highest semiconducting purity of 99.8% can be deduced based on the electrical meas-

urements (For details see the Supporting Information).<sup>[4]</sup> The high purity of s-SWNTs can be attributed to the structures of the TiC and TiO catalysts, both facilitating the nucleation of the semiconducting tubes.

### 3. Conclusion

In summary, a spatially confined strategy for the growth of high-density, horizontally aligned SWNT arrays was developed by setting a sub-10  $\mu\text{m}$  confined space in Ti-FSCVD system. The catalyst nanoparticles in the gas phase have greater chances of colliding with the substrate in the confined space, which is conducive to the deposition of nanoparticles with small sizes and good homogeneity. The confined space also helps to trap the carbon feedstock for a higher decomposition and SWNT growth efficiencies. As a result, an SWNT density of up to 65 tubes  $\mu\text{m}^{-1}$  was obtained on quartz substrates. In addition, the titanium-based catalyst TiC or TiO promotes the growth of semiconducting tubes because of the stable crystal structures and the presence of oxygen vacancies, producing a semiconducting purity of higher than 95%, locally as high as 99.8%. It is believed that through more precise design of catalysts, it will be closer to the goal of horizontally aligned SWNT arrays with high density and high

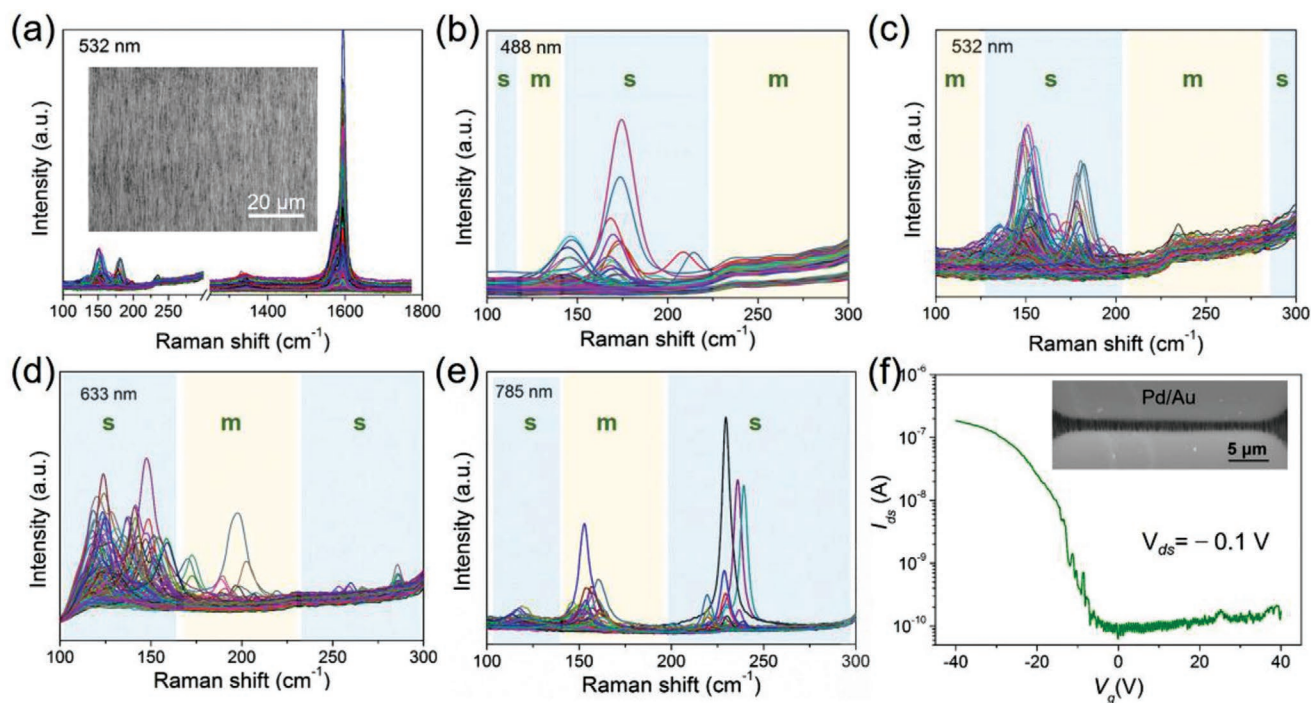


**Figure 4.** Characteristics of the high-density SWNT arrays. a) Raman line mapping spectra excited by the 532 nm laser showing the RBM, D and G bands of the SWNTs on Si/SiO<sub>2</sub> (90 nm) substrates. Inset is an SEM image of a transferred array. b–e) Raman line mapping spectra in the RBM region with excitation lasers of b) 488 nm, c) 532 nm, d) 633 nm, and e) 785 nm (scan step: 1 μm). f) A typical transfer curve of an FET based on the SWNT arrays. Inset is the SEM image of the FET.

semiconducting purity, laying a material foundation for the application of carbon nanotubes in the field of micro-nano electronics.

#### 4. Experimental Section

**Growth of SWNTs Arrays through Ti-FSCVD Method:** A multientrance quartz tube was designed for the introduction of reaction gas, catalyst precursor and catalyst promoter. The reactor furnace was operated at a set temperature of 950 °C and under atmospheric pressure in a one-inch quartz tube. Gas flowed into the reactor were controlled using mass flow controllers (MFCs). The catalyst precursor is titanocene dichloride (C<sub>10</sub>H<sub>10</sub>TiCl<sub>2</sub>) and the catalyst promoter is ferrocene (C<sub>10</sub>H<sub>10</sub>Fe). 4 mm × 6 mm sized ST-cut quartz substrates were annealed at 900 °C for 8 h and then placed at different positions in the tube with polished surfaces upward. 300 sccm argon was first introduced into the tube from entrance 1 until the temperature reached 950 °C. Titanocene dichloride powder was heated by an external heater (≈190 °C) with argon gas (150 sccm) flew through from entrance 2 and ferrocene was introduced by 50 sccm argon gas at room temperature from entrance 3. Then, Hydrogen (200–500 sccm) and ethylene (1.0 sccm) was introduced into the reactor for SWNT growth. After growth for 40–60 min, the furnace was cooled to room temperature in an argon and hydrogen atmosphere.

**Growth of SWNTs Arrays through Spatially confined Method:** The growth procedure was the same as the Ti-FSCVD, except for the placing mode of quartz substrates. In spatially confined growth, a ST-cut quartz substrate was put upside down onto another substrate (quartz or Si/SiO<sub>2</sub>) to build a narrow gap between them. Two quartz weights with weight of 3.30 g were used to press onto the quartz to further decrease the gap. After a typical growth time of 40–60 min, the furnace was cooled to room temperature in a protection atmosphere and the quartz substrates with SWNT arrays were ready for further characterization.

**TEM Characterization of Catalyst Nanoparticles:** As for the TEM samples, the preparation process is the same as spatially confined growth after replacing the quartz substrates into 10-nm-thick SiN<sub>x</sub> grids. The HRTEM images, ADF-STEM images as well as EDS mapping were conducted on an aberration-corrected TITAN Cubed Themis G2 300 equipped with Bruker QUANTAX EDS spectrometer under an accelerating voltage of 300 kV. The convergence semiangle was 21.4 mrad, and collection angle was 39–200 mrad. The beam current was typically about 30 pA when acquiring ADF-STEM images, and a larger beam current value (about 200 pA) was used for EDX mapping to improve the signal-to-noise ratio.

**General Characterization:** XPS were performed on an AXIS Supra X-ray Photoelectron Spectrometer (Kratos Analytical Ltd.) with Al Kα (1486.6 eV) as the X-ray source. SEM images were obtained on a Hitachi S4800 SEM operated at 1.0 kV. Raman spectra of SWNTs were collected by Jovin Yvon-Horiba LabRam systems with four excitation lasers: 488, 532, 633, and 785 nm. The samples are SWNT arrays transferred from quartz substrates to Si/SiO<sub>2</sub> (90 nm) substrates. Line mapping measurements were conducted with a scan step of 1 μm. AFM images were obtained using a Dimension Icon microscope (Bruker).

#### Supporting Information

Supporting Information is available from the Wiley Online Library or from the author.

#### Acknowledgements

This work was financially supported by the Ministry of Science and Technology of China (2016YFA0200100 and 2018YFA0703502), the National Natural Science Foundation of China (Grant Nos. 52021006, 51720105003, 21790052, 21974004), the Strategic Priority Research

Program of CAS (XDB36030100), and the Beijing National Laboratory for Molecular Sciences (BNLMS-CXTD-202001). The numerical calculations in this work have been done on the supercomputing system in the Supercomputing Center of Wuhan University.

## Conflict of Interest

The authors declare no conflict of interest.

## Data Availability Statement

Research data are not shared.

## Keywords

confined space, high density, horizontal arrays, semiconducting tubes, single-walled carbon nanotubes

Received: July 10, 2021

Revised: September 4, 2021

Published online:

- 
- [1] L. Qian, Y. Xie, S. Zhang, J. Zhang, *Matter* **2020**, *3*, 664.  
[2] G. Hills, C. Lau, A. Wright, S. Fuller, M. D. Bishop, T. Srimani, P. Kanhaiya, R. Ho, A. Amer, Y. Stein, D. Murphy, Arvind, A. Chandrakasan, M. M. Shulaker, *Nature* **2019**, *572*, 595.  
[3] M. F. L. De Volder, S. H. Tawfick, R. H. Baughman, A. J. Hart, *Science* **2013**, *339*, 535.  
[4] L. Liu, J. Han, L. Xu, J. Zhou, C. Zhao, S. Ding, H. Shi, M. Xiao, L. Ding, Z. Ma, C. Jin, Z. Zhang, L.-M. Peng, *Science* **2020**, *368*, 850.  
[5] M. M. Shulaker, G. Hills, N. Patil, H. Wei, H.-Y. Chen, H. S. P. Wong, S. Mitra, *Nature* **2013**, *501*, 526.  
[6] A. D. Franklin, *Nature* **2013**, *498*, 443.  
[7] S. W. Hong, T. Banks, J. A. Rogers, *Adv. Mater.* **2010**, *22*, 1826.  
[8] W. Liu, S. Zhang, L. Qian, D. Lin, J. Zhang, *Carbon* **2020**, *157*, 164.  
[9] Y. Hu, L. Kang, Q. Zhao, H. Zhong, S. Zhang, L. Yang, Z. Wang, J. Lin, Q. Li, Z. Zhang, L. Peng, Z. Liu, J. Zhang, *Nat. Commun.* **2015**, *6*, 6099.  
[10] L. Kang, Y. Hu, H. Zhong, J. Si, S. Zhang, Q. Zhao, J. Lin, Q. Li, Z. Zhang, L. Peng, J. Zhang, *Nano Res.* **2015**, *8*, 3694.  
[11] S. Zhang, Y. Hu, J. Wu, D. Liu, L. Kang, Q. Zhao, J. Zhang, *J. Am. Chem. Soc.* **2015**, *137*, 1012.  
[12] J. Wang, X. Jin, Z. Liu, G. Yu, Q. Ji, H. Wei, J. Zhang, K. Zhang, D. Li, Z. Yuan, J. Li, P. Liu, Y. Wu, Y. Wei, J. Wang, Q. Li, L. Zhang, J. Kong, S. Fan, K. Jiang, *Nat. Catal.* **2018**, *1*, 326.  
[13] D. Lin, Y. Yu, L. Li, M. Zou, J. Zhang, *Small* **2021**, *17*, 2006605.  
[14] S. Zhang, L. Kang, X. Wang, L. Tong, L. Yang, Z. Wang, K. Qi, S. Deng, Q. Li, X. Bai, F. Ding, J. Zhang, *Nature* **2017**, *543*, 234.  
[15] F. Yang, X. Wang, D. Zhang, J. Yang, D. Luo, Z. Xu, J. Wei, J.-Q. Wang, Z. Xu, F. Peng, X. Li, R. Li, Y. Li, M. Li, X. Bai, F. Ding, Y. Li, *Nature* **2014**, *510*, 522.  
[16] L. Qian, Y. Xie, Y. Yu, S. Wang, S. Zhang, J. Zhang, *Angew. Chem., Int. Ed.* **2020**, *59*, 10884.  
[17] X. Xu, Z. Zhang, L. Qiu, J. Zhuang, L. Zhang, H. Wang, C. Liao, H. Song, R. Qiao, P. Gao, Z. Hu, L. Liao, Z. Liao, D. Yu, E. Wang, F. Ding, H. Peng, K. Liu, *Nat. Nanotechnol.* **2016**, *11*, 930.  
[18] P. K. Mohapatra, S. Deb, B. P. Singh, P. Vasa, S. Dhar, *Appl. Phys. Lett.* **2016**, *108*, 042101.  
[19] X. Song, J. Gao, Y. Nie, T. Gao, J. Sun, D. Ma, Q. Li, Y. Chen, C. Jin, A. Bachmatiuk, M. H. Rummeli, F. Ding, Y. Zhang, Z. Liu, *Nano Res.* **2015**, *8*, 3164.  
[20] J. Pang, R. G. Mendes, P. S. Wrobel, M. D. Wlodarski, H. Q. Ta, L. Zhao, L. Giebeler, B. Trzebicka, T. Gemming, L. Fu, Z. Liu, J. Eckert, A. Bachmatiuk, M. H. Rummeli, *ACS Nano* **2017**, *11*, 1946.  
[21] Z. Wang, Q. Zhao, J. Zhang, *J. Phys. Chem. C* **2018**, *122*, 24823.  
[22] A. A. Rempel, W. Van Renterghem, A. A. Valeeva, M. Verwerft, S. Van den Berghe, *Sci. Rep.* **2017**, *7*, 10769.  
[23] L. Kang, Y. Hu, L. Liu, J. Wu, S. Zhang, Q. Zhao, F. Ding, Q. Li, J. Zhang, *Nano Lett.* **2015**, *15*, 403.